
Entanglement Entropy of Annulus in Holographic Thermalization ^{*}

Yi Ling ^{1,2} Yuxuan Liu ^{1,2} Zhuo-Yu Xian ³

¹ Institute of High Energy Physics, Chinese Academy of Sciences, Beijing 100049, China

² School of Physics, University of Chinese Academy of Sciences, Beijing 100049, China

³Institute of Theoretical Physics, Chinese Academy of Science, Beijing 100190, China

Abstract: The thermalization process of the holographic entanglement entropy (HEE) of an annular domain is investigated over the Vaidya-AdS geometry. We numerically determine the Hubeny-Rangamani-Takayanagi (HRT) surface which may be a hemi-torus or two disks, depending on the ratio of the inner radius to the outer radius of the annulus. More importantly, for some fixed ratio of two radii, it undergoes a phase transition or double phase transitions from a hemi-torus configuration to a two-disk configuration, or vice versa, during the thermalization. The occurrence of various phase transitions is determined by the ratio of two radii of the annulus. The rate of entanglement growth is also investigated during the thermal quench. The local maximal rate of entanglement growth occurs in the region with double phase transitions. Finally, if the quench process is fairly slow which may be controlled by the thickness of null shell, the region with double phase transitions vanishes.

Key words: holographic entanglement entropy, thermal quench, annulus

PACS: 11.25Tq

1 Introduction

Entanglement entropy, as a vital tool to measure the entanglement between quantum systems, has been extensively investigated in recent years. For a strongly coupled quantum system which is in a pure state, the entanglement entropy between the subsystem \mathcal{A} and its complement $\bar{\mathcal{A}}$ is proportional to the area of the boundary $\partial\mathcal{A}$ to the leading order [1]. In the context of AdS/CFT correspondence [2–4], the Ryu-Takayanagi (RT) formula [5, 6] conjectures that the entanglement entropy can be evaluated by the area of the minimal surface $\gamma_{\mathcal{A}}$ in the bulk which is homologous to the subregion \mathcal{A} on the boundary. Such a surface is also called RT surface or its covariant version, HRT surface [7]. In literature, the RT formula has been extensively testified in various holographic models and has been specifically computed for the subregion with a variety of shapes [8, 9]. In particular, its significant role in diagnosing the quantum critical phenomena in strongly coupled systems has been disclosed in [10–21].

Investigating the dynamical behavior of the response such as entanglement entropy by perturbing the system away from the equilibrium state is very crucial for characterizing the feature of a non-equilibrium system. A simple case is the evolution of a system after a quench process, which can be realized by turning on an external source for a short time. As a result, the system will be excited and subsequently equilibrates under evolution. In the holographic duality, the thermal quench can be modeled by Vaidya-AdS geometry, which describes the collapsing process of a null shell, which initially falls from the boundary of AdS to the bulk and eventually forms a Schwarzschild-AdS (SAdS) black brane.

In literature, the evolution behavior of HEE during such a quench process has previously been studied in [22–33], for a subregion with the shape of strip and disk. For an annular subsystem \mathcal{A} , the research on its thermalization process is still lacking. Previously, the HEE for such subregion has been computed for a static background [34, 35]. It is interesting to notice that there exist two possible configurations for the HRT surface. One has the hemi-torus shape [36, 37] while the other has the two-disk shape [38–40]. Which configuration the HRT surface takes depends on the ratio of the inner radius to the outer radius of the annulus. Moreover, the rate of entanglement growth is captured by the “entanglement tsunami” diagram [25, 27], which treats the null shell as an entanglement wave entangling the region \mathcal{A} with the outside. Since the growth rate generally depends on the ratio of two radii, it is

^{*} We are very grateful to Li Li, Chao Niu, Qiang Wen and Cheng-Yong Zhang for helpful discussions and suggestions. This work is supported by the Natural Science Foundation of China under Grant No. 11575195, 11875053 (Y.L.) and 11847229 (Z.-Y.X.). Y.L. also acknowledges the support from 555 talent project of Jiangxi Province. Z.-Y.X. also acknowledges the support from the National Postdoctoral Program for Innovative Talents BX20180318.

1) E-mail: lingyi@ihep.ac.cn

2) E-mail: liuyuxuan@ihep.ac.cn

3) E-mail: xianzy@itp.ac.cn

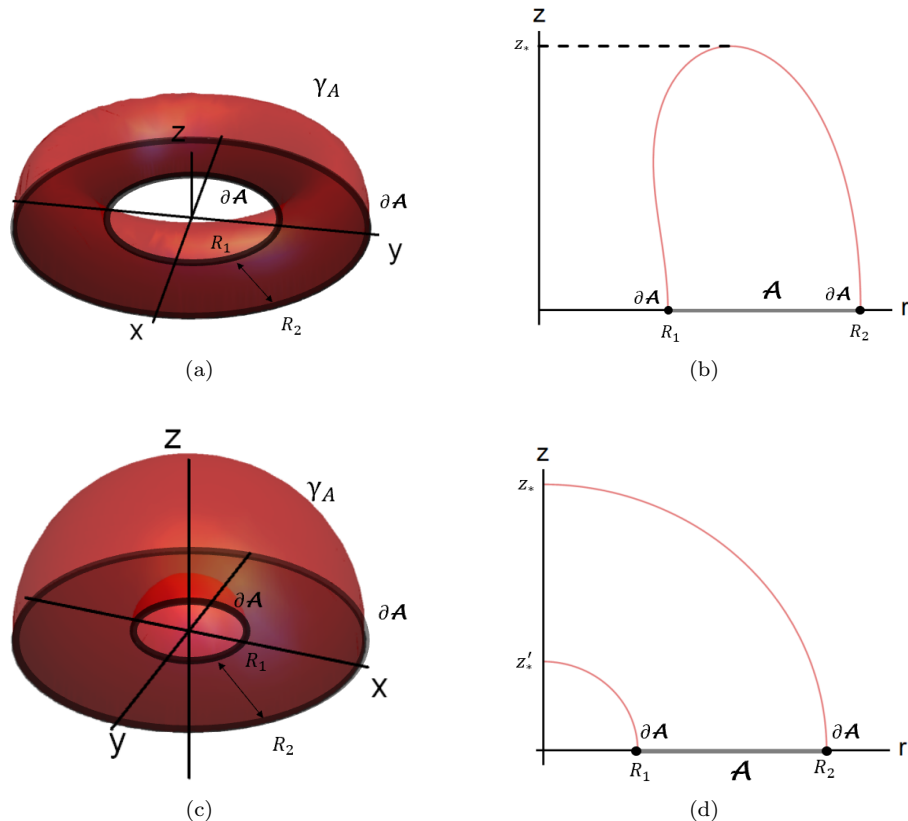


Fig. 1. Fig.1(a) illustrates the extremal surface $\gamma_{\mathcal{A}}$ in the hemi-torus shape. Fig.1(b) is its cross section after suppressing the θ direction. While Fig. 1(c) illustrates the extremal surface $\gamma_{\mathcal{A}}$ in the two-disk shape and Fig.1(d) is its cross section after suppressing the θ direction.

intriguing to investigate the phase transition of the HRT surface $\gamma_{\mathcal{A}}$ as well as the maximal rate of entanglement growth during the holographic quench process.

The paper is organized as follows. In Sec.2, we introduce the setup for the Vaidya-AdS background. The integral expressions for the area of the HRT surface will be derived for a subregion with the shape of annulus, and in the pure AdS background, the mutual information across the annular subsystem \mathcal{A} will be briefly discussed. In Sec.3, we present our numerical results for the time dependence of the HEE during the quench. In addition, various phase transitions will be illustrated in detail. The maximal rate of entanglement growth in each case and the dependence on the thickness of the shell will also be discussed. Sec.4 is our conclusion and discussions.

2 The Setup

In this section, we firstly introduce the Vaidya-AdS₄ metric, which describes the geometry of collapsing a null shell falling from the boundary to form a SAdS black hole. Then we will derive the expression of the area functional of an annular domain \mathcal{A} . For intuition, we will demonstrate two possible configurations of HRT surface $\gamma_{\mathcal{A}}$ in the pure AdS₄ case. Finally, we will discuss the characteristics of mutual information across the annulus.

2.1 Vaidya-AdS₄ background

Consider the Vaidya-AdS₄ metric in the Eddington-Finkelstein coordinates

$$ds^2 = \frac{1}{z^2} (-f(v, z)dv^2 - 2dv dz + dr^2 + r^2 d\theta^2), \quad (1)$$

with

$$f(v, z) = 1 - \frac{M}{2} \left(1 + \tanh \frac{v}{v_0} \right) z^3,$$

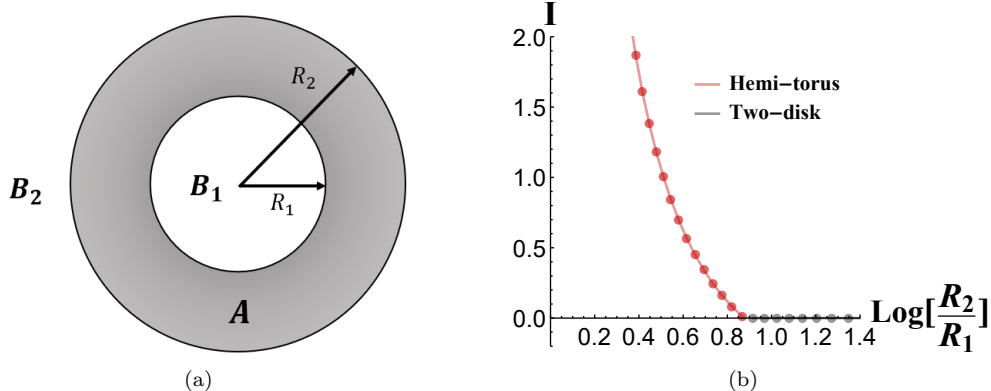


Fig. 2. As shown in Fig.2(a), \mathcal{A} represents the subsystem we investigate, while \mathcal{B}_1 and \mathcal{B}_2 are two disjoint subsystems separated by \mathcal{A} . In Fig.2(b), the holographic mutual information I between \mathcal{B}_1 and \mathcal{B}_2 is plotted with different ratio of two radii R_1 and R_2 in the AdS₄ background. The phase transition occurs at $R_2/R_1 \approx 2.4$.

where we have set the AdS radius $R_{AdS} = 1$. M characterizes the mass of the black hole and v_0 labels the thickness of the null shell. In this setup, the coordinate v labels the boundary time t when $z \rightarrow 0$. Moreover, in the limit of $v \rightarrow -\infty$, the metric in (1) approaches

$$f(v, z) = 1,$$

which is the AdS metric, while in the limit of $v \rightarrow \infty$, the metric approaches

$$f(v, z) = 1 - Mz^3,$$

which is just the metric on the SAdS spacetime.

2.2 HRT surface $\gamma_{\mathcal{A}}$ of an annular domain \mathcal{A}

On the boundary, consider the subregion $\mathcal{A}(r, \theta)$ which is an annulus with $r \in [R_1, R_2]$ and $\theta \in (0, 2\pi]$. Due to the spherical symmetry, the region \mathcal{A} is completely specified by the radius r . Then the corresponding area of the extremal surface $\gamma_{\mathcal{A}}$ anchored on $\partial\mathcal{A}$ is described by

$$z = z(r), \quad v = v(r)$$

and reads as

$$A[\gamma_{\mathcal{A}}] = 2\pi \int_{R_1}^{R_2} dr \frac{r}{z^2} \sqrt{1 - 2v'z' - f(v, z)v'^2}. \quad (2)$$

The equations of motion are obtained by extremizing the area functional (2). It is noticed that as the inner radius $R_1 \rightarrow 0$, the above area functional reduces to the functional corresponding to a spherical region \mathcal{A} with radius R_2 (see [22, 25, 28]).

Before the thermal quench, the geometry is a pure AdS₄ spacetime and the corresponding area functional reduces to

$$A[\gamma_{\mathcal{A}}] = 2\pi \int_{R_1}^{R_2} dr \frac{r}{z^2} \sqrt{1 + z'^2}. \quad (3)$$

The phase transition of HRT surface in AdS₄ spacetime has been investigated in literature. As the ratio of the outer radius R_2 to the inner radius R_1 approaches one, the HRT surface is in the hemi-torus phase (Fig.1(a)). Then decreasing the inner radius R_1 , as the ratio $R_2/R_1 \rightarrow 2.4$ [35], the configuration of the HRT surface will undergo a phase transition from the hemi-torus phase to the two-disk phase (Fig.1(c)).

2.3 Mutual information

Mutual information between two disjoint subsystems B_1 and B_2 is defined as

$$I(B_1; B_2) \equiv S(B_1) + S(B_2) - S(B_1 \cup B_2) \geq 0 \quad (4)$$

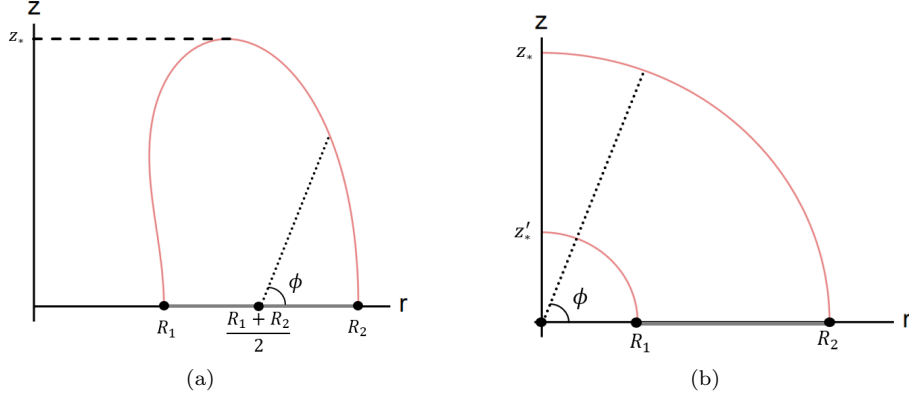


Fig. 3. The parameterization of the HRT surface. If the HRT surface is in the hemi-torus phase, the parameter ϕ is shown in Fig.3(a) with $0 \leq \phi \leq \pi$. While if the HRT surface is in the two-disk phase, the parameter is shown in Fig.3(b) with $0 \leq \phi \leq \frac{\pi}{2}$.

Specifically, for an annular subregion \mathcal{A} of the boundary, we take \mathcal{B}_1 and \mathcal{B}_2 as two disjoint subsystems, which are located in $r \leq R_1$ and $r \geq R_2$ respectively as shown in Fig.2(a).

In the holographic setup, when decreasing the inner radius R_1 with fixed R_2 , the mutual information between \mathcal{B}_1 and \mathcal{B}_2 decreases monotonically to zero, which is consistent with the result in literature [8, 34, 35]. Furthermore, the HRT surface $\gamma_{\mathcal{A}}$ corresponding to the annulus \mathcal{A} is in the hemi-torus phase as $I(\mathcal{B}_1; \mathcal{B}_2) > 0$, while it is in the two-disk phase as $I(\mathcal{B}_1; \mathcal{B}_2) = 0$ as shown in Fig.2(b).

For a general quantum system, mutual information measures the entanglement and correlations between the subsystems and gives an upper bound for the correlations as well. Therefore, for a system in pure state, if a HRT surface \mathcal{A} is in the hemi-torus phase, the d.o.f. of the subsystem \mathcal{B}_1 are generally entangled with those of the subsystem \mathcal{B}_2 . While, if the HRT surface $\gamma_{\mathcal{A}}$ is in the two-disk phase, there is no entanglement between them.

So far, we have derived the integral expressions of the entanglement entropy between the subsystem \mathcal{A} and its complement and discussed the mutual information across the subsystem \mathcal{A} in pure AdS₄ spacetime. In the next section, we will investigate the evolution of the HEE in the Vaidya-AdS₄ spacetime.

3 Numeric Method

First of all, to get rid of ultra-violet (UV) divergence at $z \rightarrow 0$, we only consider the finite term in (2), which is

$$A_{Ren} = A[\gamma_{\mathcal{A}}] - \frac{R_1 + R_2}{\epsilon}, \quad (5)$$

where ϵ is the UV cut-off. It is manifest that A_{Ren} is cut-off independent. Then we fix all the free parameters: the mass $M = 1$, the thickness of the shell $v_0 = 0.3$, the outer radius of the annulus $R_2 = 5$ and the inner radius $R_1 \in [0.5, 4.5]$.

Specifically, the extremal surface $\gamma_{\mathcal{A}}$ is parameterized by

$$z = z(\phi), \quad r = r(\phi), \quad v = v(\phi), \quad (6)$$

where ϕ is the polar angle as shown in Fig.3. Since above three variables in (6) are not independent, it is necessary to introduce a constraint equation. In the hemi-torus phase, the constraint equation is

$$z(\phi) \cos(\phi) - \left(r(\phi) - \frac{R_1 + R_2}{2} \right) \sin(\phi) = 0, \quad (0 \leq \phi \leq \pi) \quad (7)$$

and the boundary conditions are

$$z(0) = z(\pi) = 0, \quad v(0) = v(\pi) = t, \quad r(0) = R_2, \quad r(\pi) = R_1.$$

While in the two-disk phase, the constraint equation is

$$z(\phi) \cos(\phi) - r(\phi) \sin(\phi) = 0, \quad (0 \leq \phi \leq \frac{\pi}{2}) \quad (8)$$

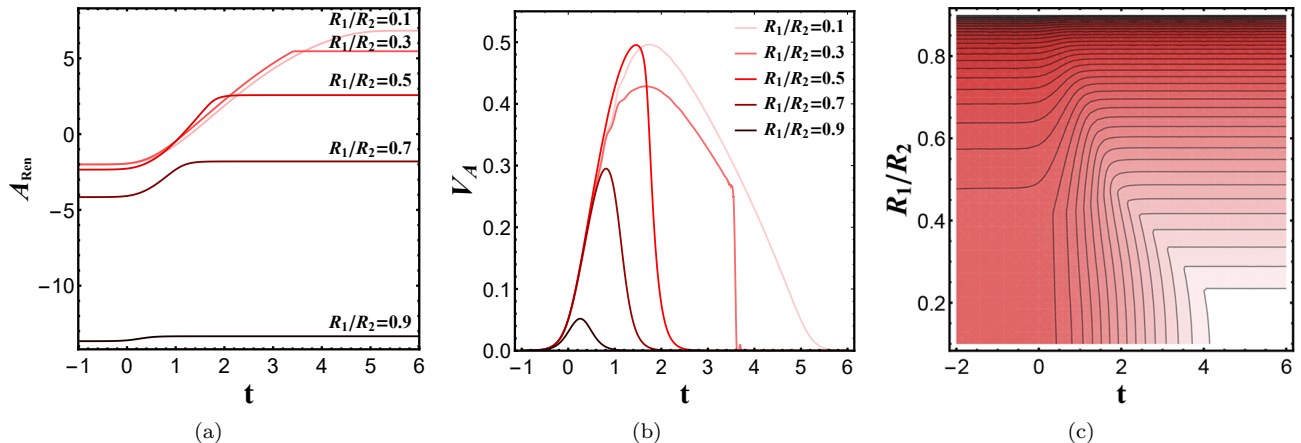


Fig. 4. Fig.4(a) illustrates the evolution of the HEE with $R_1/R_2 = 0.1, 0.3, 0.5, 0.7$ and 0.9 , respectively, while Fig.4(b) illustrates the rate of the entanglement growth in the unit of the length of $\partial\mathcal{A}$. Fig.4(c) is the contour plotting of HEE during the evolution with different ratio R_1/R_2 . The lighter the color is, the larger the value of HEE is.

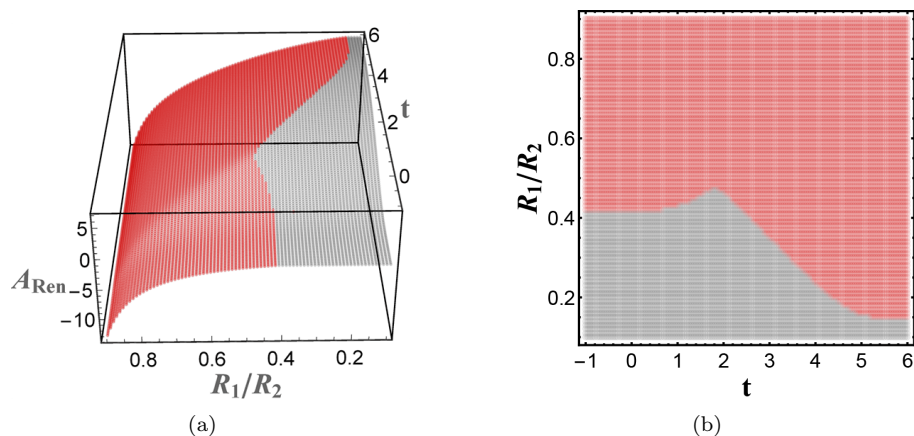


Fig. 5. The evolution of HEE with different R_1/R_2 is shown in Fig.5(a). The data in red indicate that the HRT surface is in the hemi-torus phase, while the data in grey indicate that the HRT surface is in the two-disk phase. Fig.5(b) is obtained by projecting the result in Fig.5(a) onto the $(R_1/R_2, t)$ plane, which is convenient for us to identify the phase corresponding to the parameter R_1/R_2 at any moment.

and the boundary conditions reduce to

$$z(0) = z'(\frac{\pi}{2}) = 0, \quad v(0) = t, \quad v'(\frac{\pi}{2}) = 0, \quad r(0) = R_2 \text{ (or } R_1), \quad r(\frac{\pi}{2}) = 0.$$

The above constraint equations (7) and (8) are imposed to the area functional (2) by the method of lagrange multiplier. Then, the corresponding E.O.M. can be numerically solved by the method of finite differences.

Next we turn to present the numeric results for the evolution of the HEE based on renormalized area A_{Ren} . Firstly, we are concerned with the time dependence of the HEE for different ratio of two radii R_1/R_2 , as illustrated in Fig.4(a). It is obvious to find that the entanglement entropy is always increasing roughly with a linear manner* with time at the intermediate stage of the thermal quench and finally saturates. Moreover, defining the rate of entanglement growth as

$$V_{\mathcal{A}} = \frac{1}{R_1 + R_2} \frac{dA_{Ren}}{dt},$$

we find it always increases with time at the early stage and eventually decreases to zero at equilibrium as shown in

*The linearity is not quite precise here for small R_1/R_2 as shown in Fig.4(b), but in general, the larger the size of the region \mathcal{A} is, the more obvious the stage of linear growth is.

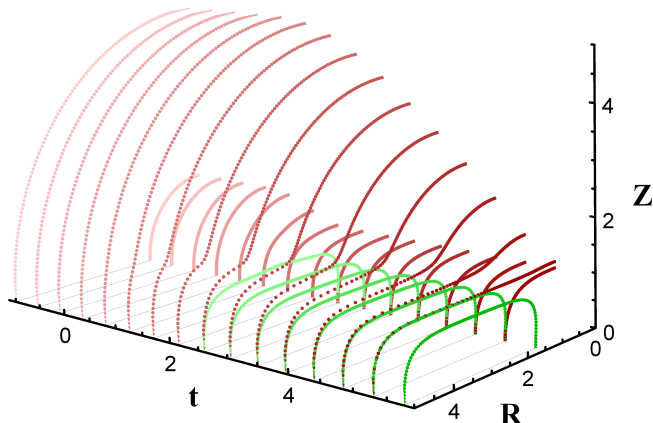


Fig. 6. Two candidates of the HRT surface anchored on the $\partial\mathcal{A}$ are shown in the figure. At each moment during the evolution, the candidate in the two-disk phase is plotted in red, while the candidate in the hemi-torus phase is plotted in green. Note that the HRT surface will not exactly lie on a time slice during the evolution, but the figure is good enough for us to gain intuition.

Fig.4(b). In general, the saturation value as well as the saturation time is increasing with the width of the region \mathcal{A} , which are quite common phenomena in literature. Because the HRT surface with the wider boundary region \mathcal{A} usually stretches deeper into the bulk region, the null shell also takes longer time to reach this region during the holographic quench process. As a consequence, it takes longer time to get saturation. Furthermore, the saturation time approaches a constant as the ratio $R_1/R_2 \rightarrow 0$ as shown in Fig.4(c). This result indicates that in the region where R_1/R_2 approaches zero, the HRT surfaces with the different R_1 are in the two-disk phase near saturation. Since the outer radius R_2 is fixed in the setting, all the HRT surfaces which are in the two-disk phase share the same outer part of extremal surface as well as the saturation time.

It is noticed that the evolution of HEE undergoes an unsmooth saturation while $R_1/R_2 = 0.3$. This result reveals that the HRT surface undergoes a phase transition during the thermal quench. Meanwhile, other results in Fig.4(a) and 4(b) demonstrate that the HRT surfaces always in the same phase during the quench. We will analyze these results with more details in the next subsection.

3.1 Phase transition of the HRT surface

In Fig.5(a) we demonstrate the time evolution of HEE under different inner radius R_1 . The region marked in red represents the HRT surface in the hemi-torus phase, while the region in gray represents the HRT surface in the two-disk phase. In general, the HRT surfaces are in the hemi-torus phase as the ratio of two radii R_1/R_2 approaches one, otherwise, if $R_1/R_2 \ll 1$, the HRT surfaces will be in the two-disk phase. In addition, the critical R_1 , which may be defined as the borderline of two phases, shifts non-monotonically during the thermal quench as shown in Fig.5(b). At the early stage of the quench, the critical point shifts towards the outer radius R_2 . After reaching its peak at $t \approx 1.80$, the critical point decreases monotonically to a lower level and eventually becomes stable.

The lower level of the critical point at late time can be understood from Fig.6. At the early stage, the candidate in the two-disk phase possesses a smaller area and thus is the HRT surface in consequence. As the evolution proceeds, the other candidate in the hemi-torus phase begins to compete with the candidate in the two-disk phase and eventually becomes the HRT surface at the late stage. Note that at the late stage, the candidate in the two-disk phase possesses a thin bottleneck near $R = 0$ and this will naturally lead to the candidate in hemi-torus phase becoming the HRT surface. In addition, the larger the ratio R_1/R_2 is, the earlier the thin bottleneck occurs. As a consequence, the phase transition occurs earlier during the evolution.

It is interesting to notice that for a fixed ratio R_1/R_2 , the phase transition occurs during the thermal quench. Further, the times of phase transition depend on the specific value of the ratio. According to this, the evolution of HEE during the quench process can be characterized by the following three distinct types.

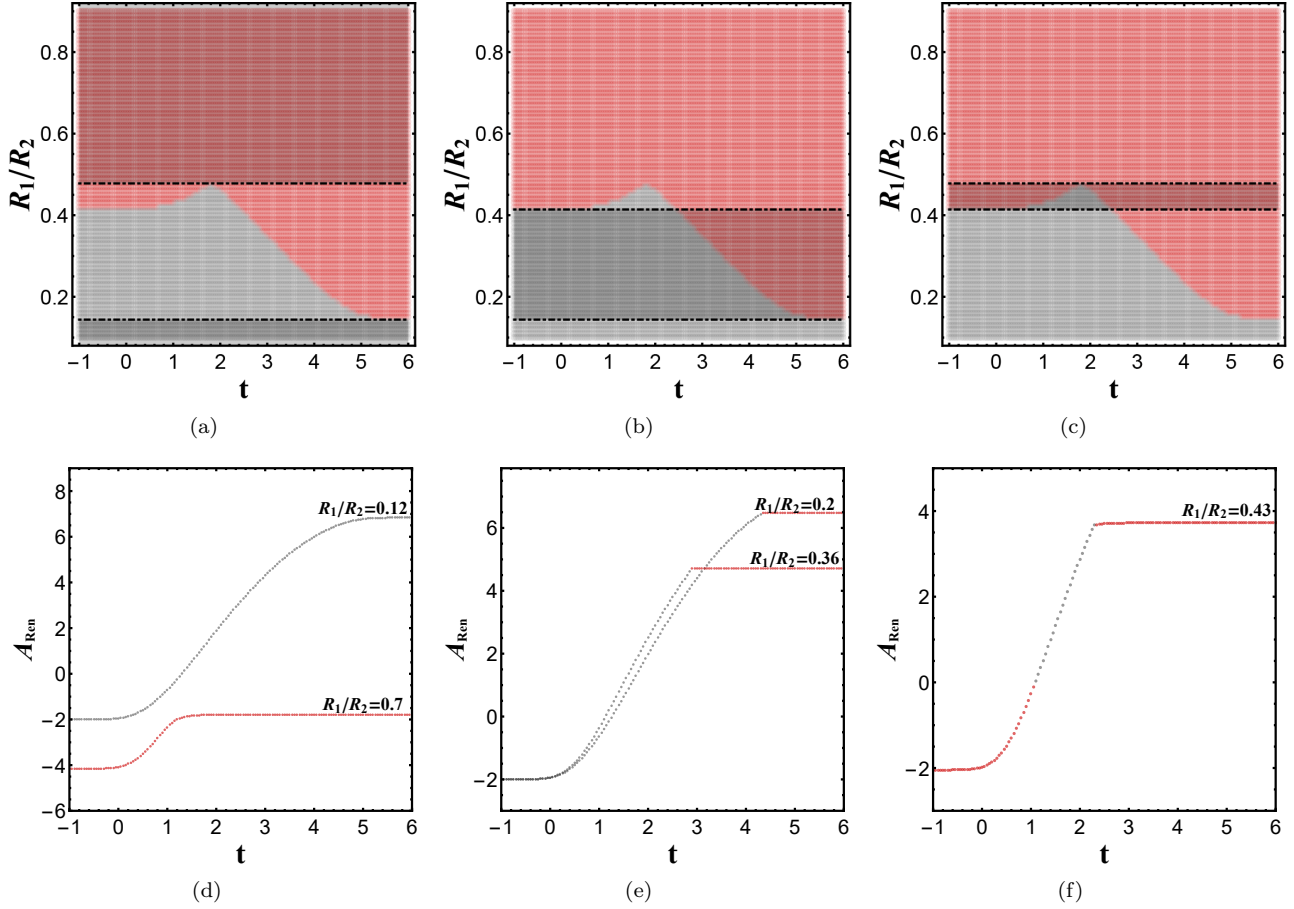


Fig. 7. The shadow regions in Fig.7(a), Fig.7(b) and Fig.7(c) represent the region with no phase transition, single phase transition and double phase transitions respectively, during the evolution of HEE with fixed R_1/R_2 . The curves in grey exhibit the evolution of HEE in the two-disk phase while the curves in red exhibit the evolution of HEE in the hemi-torus phase.

- Region with no phase transition

For the ratio $R_1/R_2 \geq 0.48$, the HRT surface is always in the hemi-torus phase during the quench process, while for the ratio $R_1/R_2 \leq 0.14$, the HRT surface is always in the two-disk phase as shown in Fig.7(a). Note that without phase transition, the evolution of HEE of an annular domain is similar to that of a ball-shaped domain [22, 26], as the evolution curve is always smooth (Fig.7(d)). Moreover, the subsystem \mathcal{A} with greater $R_2 - R_1$ generally possesses a greater saturation value and longer saturation time as discussed before.

- Region with single phase transition

For the ratio $0.14 \leq R_1/R_2 \leq 0.42$, the HRT surface is in the two-disk phase at the early stage of evolution, then it will undergo a phase transition to the hemi-torus phase and persist all the way to saturation as shown in Fig.7(b). In addition, the critical point decreases almost linearly with time t and ultimately reaches a global minimum which is consistent with the critical point in the Schwarzschild-AdS geometry.

When the system approaches the critical point, the first derivative of the HEE with respect to time t is discontinuous (Fig.7(e)). Similarly, in this region both the saturation value and the saturation time are generally increasing with $R_2 - R_1$. During the evolution, the discontinuity of the derivative of HEE with respect to time is discussed mostly when the boundary region \mathcal{A} is a strip and the width of the strip is greater than the event horizon. The difference is that when the boundary \mathcal{A} is a strip, the discontinuity occurs due to the multiple values of the extremal surface [22, 26, 29, 30], but when the boundary region \mathcal{A} is an annulus, the discontinuity occurs due to the phase transition from the two-disk phase to the hemi-torus phase.

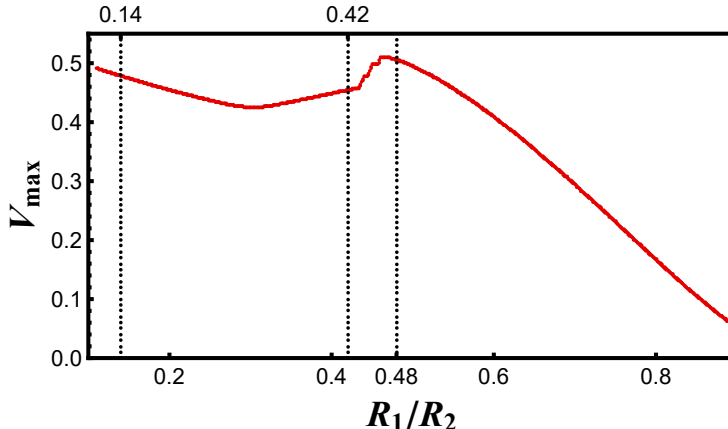


Fig. 8. The maximal rate of entanglement growth V_{max} with different ratios of two radii R_1/R_2 is plotted in red. Three dashed lines divide the whole phase diagram into three distinct regions as discussed in Sec.3.1.

- Region with double phase transitions

For the ratio $0.42 \leq R_1/R_2 \leq 0.48$, it is interesting to notice that there is a peak for the borderline of two phases, therefore, in this region the HRT surface will change its phase twice when R_1/R_2 is fixed, as shown in Fig.7(c). At the early stage of evolution, the HRT surface is in the hemi-torus phase and at the intermediate stage, it undergoes the first phase transition from the hemi-torus phase to the two-disk phase. Eventually, the HRT surface will undergo the second phase transition to the original hemi-torus phase and will persist all the way to equilibrium.

It is also intriguing to notice that when the system approaches the first critical point (at which the phase changes from the hemi-torus phase to the two-disk phase), the time derivative of HEE seems to be continuous and this is different from the behavior of the system at the second critical point as shown in Fig.7(f). When the HRT surface undergoes the second phase transition, the time derivative of HEE is discontinuous, which is consistent with the result in the region with single phase transition. Furthermore, after passing through the second critical point, the system does not reach the equilibrium immediately. This phenomenon is in contrast to the strip case, in which the discontinuity only occurs at the equilibrium.

After identifying three distinct regions during the evolution of HEE, we are wondering how the entanglement growth is characterized by these regions and how the different values of the parameters could affect these regions. Therefore, in the next two subsections, we will explore the dependence of the rate of the entanglement growth $V_{\mathcal{A}}$ on the ratio of two radii R_1/R_2 as well as the dependence of the evolution of HEE on the thickness v_0 of the null shell.

3.2 Maximal rate of the entanglement growth V_{max}

As discussed in [25, 27], the rate of linear growth at the intermediate stage provides a geometric interpretation of the entanglement growth: during the thermal quench, there is a wave propagating inward from the boundary of \mathcal{A} . The region which has been covered by the wave is entangled with the region outside \mathcal{A} , while the region which has not been covered is generally not entangled with the outside. Naturally, when the wave covers the whole region \mathcal{A} , the saturation occurs. This phenomenon is called “entanglement tsunami” in literature and the speed of the tsunami is characterized by the maximal rate of the entanglement growth V_{max} during the evolution.

Furthermore, we point out that the dependence of the tsunami speed V_{max} on the ratio R_1/R_2 exhibits distinct behaviors in regions with different phase transitions, as shown in Fig.8. In the region with no phase transition ($R_1/R_2 \leq 0.14 \cup R_1/R_2 \geq 0.48$), the tsunami speed V_{max} always decreases with the ratio R_1/R_2 . In particular, when the ratio $R_1/R_2 \rightarrow 1$, the maximal rate of entanglement growth V_{max} decreases to zero. In the region with single phase transition ($0.14 \leq R_1/R_2 \leq 0.42$), the tsunami speed V_{max} decreases linearly at first and increases again after reaching a local minimum, while in the region with double phase transitions ($0.42 \leq R_1/R_2 \leq 0.48$), the speed of entanglement tsunami reaches a local maximum. This reveals that the wave-front shifts with a fast rate from the boundary $\partial\mathcal{A}$ in the region with double phase transitions. Moreover, in a relativistic system, it is natural to expect that the maximal rate of entanglement growth is constrained by the causality. In this paper, the fastest rate of entanglement tsunami occurs at $t \approx 0.46$, $V_{max} = 0.51$, which is smaller than the speed of light. The result is consistent with the one

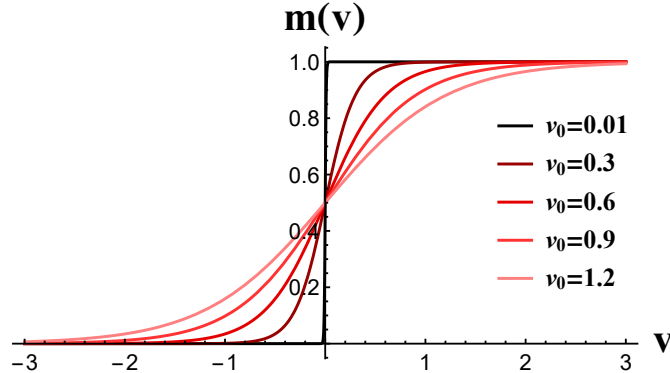


Fig. 9. The evolution of the mass function $m(v)$ indicates it usually increases rapidly with small v_0 .

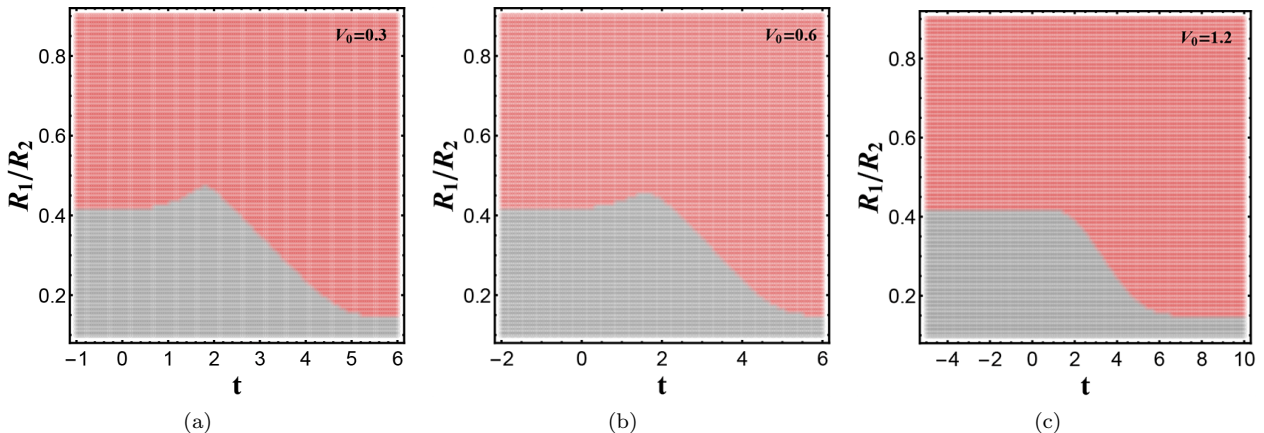


Fig. 10. The evolution of HEE with various values of parameter v_0 . The red region represents the HRT surface in the hemi-torus phase, while the grey region represents the HRT surface in the two-disk region.

in [25, 27], which exhibit a global maximal growth rate of the 4-dimensional SAdS case under the limit of rapid quenching.

3.3 Variation of the thickness v_0 of the null shell

The thickness of the null shell v_0 also characterizes the speed of the quench. Defining the mass function $m(v)$ as

$$m(v) \equiv \frac{M}{2} \left(1 + \tanh \frac{v}{v_0} \right). \quad (9)$$

For smaller v_0 , the mass $m(v)$ of the system increases more rapidly to the final saturation, while for larger v_0 , $m(v)$ increases slowly as shown in Fig.9. Therefore, $1/v_0$ denotes the speed of the quench process: the larger the value of $1/v_0$ is, the sooner the quench saturates.

In Fig.10, we plot the evolution of HEE for various values of the parameter v_0 . The position of the critical point near equilibrium will not be affected by v_0 . For the larger v_0 , the subsystem \mathcal{A} takes longer time to reach equilibrium.

The most prominent phenomenon in Fig.10 is the size change of the region with double phase transitions. For small v_0 , the peak of the critical point is very sharp. With the increase of v_0 , the peak of the critical point decreases and eventually vanishes such that the region with double phase transitions finally disappears.

4 Conclusions and discussions

We have investigated the holographic thermalization process of an annular subsystem \mathcal{A} on the boundary over the Vaidya-AdS geometry. Two distinct configurations of HRT surface are obtained which are the hemi-torus phase and the two-disk phase. Which phase the HRT surface belongs to depends on the ratio of the inner radius to the outer

radius of the annulus. In addition, the maximal rate of the entanglement growth V_{max} exhibits distinct behavior with the different ratio of two radii.

During the thermalization process, the system with fixed R_1/R_2 possibly undergoes a phase transition or double phase transitions from a hemi-torus configuration to a two-disk configuration, or vice versa. The occurrence of various phase transitions is determined by the ratio of two radii of the annulus, which allows us to extract out three distinct regions. When the annulus is fairly wide or narrow, the HRT surface $\gamma_{\mathcal{A}}$ is always in the two-disk phase or hemi-torus phase and no phase transition occurs during the whole process, and the entanglement tsunami propagates more slowly with the larger ratio R_1/R_2 . For the ratio $0.14 \leq R_1/R_2 \leq 0.42$, the phase transition occurs one time during the thermalization, and the propagation of the entanglement tsunami reaches a local minimum. It is quite intriguing that, there exists a region that the phase transition occurs twice during the thermalization. The HRT surface is in the hemi-torus phase at the early time, in the two-disk phase at the intermediate and in the hemi-torus phase at the late time. In this region, the propagation of the entanglement tsunami reaches a local maximum, which means the entanglement grows fairly fast in the region with double phase transitions. Moreover, the local maximum we obtained is consistent with the fastest rate of entanglement growth under the fast quenching limit, which means the rate is constrained by causality. In addition, the region with double phase transitions becomes wide with a fast quench, and becomes narrow, even vanishes with a slow quench.

In this paper, we have discussed the evolution of HEE following a global quench. It is interesting to generalize our analysis to the inhomogeneous and anisotropic case. Moreover, due to the restriction of the numeric method, we have only investigated the quench with the thickness of the null shell $v_0 \geq 0.3$. It is also worthy to investigate the evolution of HEE in the thin shell limit, since the diagram of entanglement tsunami is more precise than the case with a finite thickness v_0 .

References

- 1 M. Rangamani and T. Takayanagi, “Holographic Entanglement Entropy,” Lect. Notes Phys. **931**, pp.1 (2017) [arXiv:1609.01287 [hep-th]].
- 2 J. M. Maldacena, “The Large N limit of superconformal field theories and supergravity,” Int. J. Theor. Phys. **38**, 1113 (1999) [Adv. Theor. Math. Phys. **2**, 231 (1998)] [hep-th/9711200].
- 3 S. S. Gubser, I. R. Klebanov and A. M. Polyakov, “Gauge theory correlators from noncritical string theory,” Phys. Lett. B **428**, 105 (1998) [hep-th/9802109].
- 4 E. Witten, “Anti-de Sitter space and holography,” Adv. Theor. Math. Phys. **2**, 253 (1998) [hep-th/9802150].
- 5 S. Ryu and T. Takayanagi, “Holographic derivation of entanglement entropy from AdS/CFT,” Phys. Rev. Lett. **96**, 181602 (2006) [hep-th/0603001].
- 6 S. Ryu and T. Takayanagi, “Aspects of Holographic Entanglement Entropy,” JHEP **0608**, 045 (2006) [hep-th/0605073].
- 7 V. E. Hubeny, M. Rangamani and T. Takayanagi, “A Covariant holographic entanglement entropy proposal,” JHEP **0707**, 062 (2007) [arXiv:0705.0016 [hep-th]].
- 8 P. Fonda, L. Giomi, A. Salvio and E. Tonni, “On shape dependence of holographic mutual information in AdS₄,” JHEP **1502**, 005 (2015) [arXiv:1411.3608 [hep-th]].
- 9 P. Fonda, D. Seminara and E. Tonni, “On shape dependence of holographic entanglement entropy in AdS₄/CFT₃,” JHEP **1512**, 037 (2015) [arXiv:1510.03664 [hep-th]].
- 10 C. Holzhey, F. Larsen and F. Wilczek, “Geometric and renormalized entropy in conformal field theory,” Nucl. Phys. B **424**, 443 (1994) [hep-th/9403108].
- 11 G. Vidal, J. I. Latorre, E. Rico and A. Kitaev, “Entanglement in quantum critical phenomena,” Phys. Rev. Lett. **90**, 227902 (2003) [quant-ph/0211074].
- 12 A. Kitaev and J. Preskill, “Topological entanglement entropy,” Phys. Rev. Lett. **96**, 110404 (2006) [hep-th/0510092].
- 13 P. Calabrese and J. L. Cardy, “Entanglement entropy and quantum field theory,” J. Stat. Mech. **0406**, P06002 (2004) [hep-th/0405152].
- 14 T. Grover, A. M. Turner and A. Vishwanath, “Entanglement Entropy of Gapped Phases and Topological Order in Three dimensions,” Phys. Rev. B **84**, 195120 (2011) [arXiv:1108.4038 [cond-mat.str-el]].
- 15 Y. Ling, P. Liu, J. P. Wu and Z. Zhou, “Holographic Metal-Insulator Transition in Higher Derivative Gravity,” Phys. Lett. B **766**, 41 (2017) [arXiv:1606.07866 [hep-th]].
- 16 Y. Ling, P. Liu and J. P. Wu, “Characterization of Quantum Phase Transition using Holographic Entanglement Entropy,” Phys. Rev. D **93**, no. 12, 126004 (2016) [arXiv:1604.04857 [hep-th]].
- 17 Y. Ling, P. Liu, C. Niu, J. P. Wu and Z. Y. Xian, “Holographic Entanglement Entropy Close to Quantum Phase Transitions,” JHEP **1604**, 114 (2016) [arXiv:1502.03661 [hep-th]].
- 18 H. Guo, X. M. Kuang and B. Wang, “Holographic entanglement entropy and complexity in Stückelberg superconductor,” Phys. Lett. B **797**, 134879 (2019) [arXiv:1902.07945 [hep-th]].
- 19 X. X. Zeng, H. Zhang and L. F. Li, “Phase transition of holographic entanglement entropy in massive gravity,” Phys. Lett. B **756**, 170 (2016) [arXiv:1511.00383 [gr-qc]].
- 20 X. X. Zeng and L. F. Li, “Van der Waals phase transition in the framework of holography,” Phys. Lett. B **764**, 100 (2017) [arXiv:1512.08855 [hep-th]].
- 21 X. X. Zeng, X. M. Liu and L. F. Li, “Phase structure of the Born-Infeld anti-de Sitter black holes probed by non-local observables,” Eur. Phys. J. C **76**, no. 11, 616 (2016) [arXiv:1601.01160 [hep-th]].
- 22 T. Albash and C. V. Johnson, “Evolution of Holographic Entanglement Entropy after Thermal and Electromagnetic Quenches,” New

-
- J. Phys. **13**, 045017 (2011) [arXiv:1008.3027 [hep-th]].
- 23 V. Balasubramanian *et al.*, “Thermalization of Strongly Coupled Field Theories,” Phys. Rev. Lett. **106**, 191601 (2011) [arXiv:1012.4753 [hep-th]].
- 24 V. Balasubramanian *et al.*, “Inhomogeneous Thermalization in Strongly Coupled Field Theories,” Phys. Rev. Lett. **111**, 231602 (2013) [arXiv:1307.1487 [hep-th]].
- 25 H. Liu and S. J. Suh, “Entanglement growth during thermalization in holographic systems,” Phys. Rev. D **89**, no. 6, 066012 (2014) [arXiv:1311.1200 [hep-th]].
- 26 E. Caceres and A. Kundu, “Holographic Thermalization with Chemical Potential,” JHEP **1209**, 055 (2012) [arXiv:1205.2354 [hep-th]].
- 27 H. Liu and S. J. Suh, “Entanglement Tsunami: Universal Scaling in Holographic Thermalization,” Phys. Rev. Lett. **112**, 011601 (2014) [arXiv:1305.7244 [hep-th]].
- 28 G. Camilo, B. Cuadros-Melgar and E. Abdalla, “Holographic thermalization with a chemical potential from Born-Infeld electrodynamics,” JHEP **1502**, 103 (2015) [arXiv:1412.3878 [hep-th]].
- 29 B. Chen, W. M. Li, R. Q. Yang, C. Y. Zhang and S. J. Zhang, “Holographic subregion complexity under a thermal quench,” JHEP **1807**, 034 (2018) [arXiv:1803.06680 [hep-th]].
- 30 Y. Ling, Y. Liu and C. Y. Zhang, “Holographic Subregion Complexity in Einstein-Born-Infeld theory,” Eur. Phys. J. C **79**, no. 3, 194 (2019) [arXiv:1808.10169 [hep-th]].
- 31 Y. T. Zhou, M. Ghodrati, X. M. Kuang and J. P. Wu, “Evolutions of entanglement and complexity after a thermal quench in massive gravity theory,” Phys. Rev. D **100**, no. 6, 066003 (2019) [arXiv:1907.08453 [hep-th]].
- 32 X. Bai, B. H. Lee, L. Li, J. R. Sun and H. Q. Zhang, “Time Evolution of Entanglement Entropy in Quenched Holographic Superconductors,” JHEP **1504**, 066 (2015) [arXiv:1412.5500 [hep-th]].
- 33 Y. Z. Li, S. F. Wu, Y. Q. Wang and G. H. Yang, “Linear growth of entanglement entropy in holographic thermalization captured by horizon interiors and mutual information,” JHEP **1309**, 057 (2013) doi:10.1007/JHEP09(2013)057 [arXiv:1306.0210 [hep-th]].
- 34 M. Han and Q. Wen, “Entanglement entropies from entanglement contour: annuli and spherical shells,” arXiv:1905.05522 [hep-th].
- 35 Y. Nakaguchi and T. Nishioka, “Entanglement Entropy of Annulus in Three Dimensions,” JHEP **1504**, 072 (2015) [arXiv:1501.01293 [hep-th]].
- 36 N. Drukker and B. Fiol, “On the integrability of Wilson loops in AdS(5) x S**5: Some periodic ansatze,” JHEP **0601**, 056 (2006) [hep-th/0506058].
- 37 A. Dekel and T. Klose, “Correlation Function of Circular Wilson Loops at Strong Coupling,” JHEP **1311**, 117 (2013) [arXiv:1309.3203 [hep-th]].
- 38 N. Shiba, “Entanglement Entropy of Two Black Holes and Entanglement Entropic Force,” Phys. Rev. D **83**, 065002 (2011) [arXiv:1011.3760 [hep-th]].
- 39 N. Shiba, “Entanglement Entropy of Two Spheres,” JHEP **1207**, 100 (2012) [arXiv:1201.4865 [hep-th]].
- 40 J. Cardy, “Some results on the mutual information of disjoint regions in higher dimensions,” J. Phys. A **46**, 285402 (2013) [arXiv:1304.7985 [hep-th]].
- 41 M. M. Wolf, F. Verstraete, M. B. Hastings and J. I. Cirac, “Area Laws in Quantum Systems: Mutual Information and Correlations,” Phys. Rev. Lett. **100**, no. 7, 070502 (2008) [arXiv:0704.3906 [quant-ph]].